Appl Phys B (2012) 108:353–359
DOI 10.1007/s00340-012-4975-z

Applied Physics B
Lasers and Optics

Sensitivity enhancement of off-axis ICOS using wavelength modulation

P. Malara · M.F. Witinski · F. Capasso · J.G. Anderson · P. De Natale

Received: 19 October 2011 / Revised version: 23 February 2012 / Published online: 30 March 2012

Abstract In this paper, we analyze the sensitivity enhancement attainable by combining a wavelength modulation (WM) technique to integrated cavity output spectroscopy (ICOS), pointing out how the spectrometer's parameters and the acquisition strategy affect the detection noise in both techniques. We point out that WM-ICOS is mainly limited by the slow scan rate that it requires, compared to regular ICOS. Nevertheless, according to our analysis, WM can still appreciably improve the SNR of an ultrasensitive ICOS system, if the cavity transmission is so low that the detector noise is not negligible. In light of these considerations, we directly compare the performance of ICOS and WM-ICOS in a high sensitivity ambient-air methane detection experiment, finding a good agreement with the theoretical influence of the various spectrometer parameters.

1 Introduction

Sensitivity of spectroscopic detection is a crucial issue whenever concentrations of trace molecular species have to be measured. Atmospheric chemistry, environmental monitoring, biomedical diagnostics, and molecular astrophysics are just a few examples of research areas that demand ultrasensitive and rugged setups, capable of field measurements. Off-axis Integrated Cavity Output Spectroscopy (ICOS), introduced in 2001 [1], has proven to be one of the most sensitive and robust laser-based techniques, and since its invention it has been used in many diverse applications and with a range of radiation sources [2–5].

In the last few years, a number of works have reported how introducing a wavelength modulation detection scheme in conjunction with the ICOS optical design can boost performance compared to ICOS alone [6–14]. As we show in Table 1, a wide range of SNR enhancements were obtained in the WM-ICOS attempts, corresponding to the wide range of experimental parameters reported. In particular, while an enhancement factor around 14 is demonstrated in cavities with mirror reflectivity $R = 99.8\ \%$, only a factor 5 enhancement was reported with $R = 99.975\ \%$.

Understanding the noise issues in ICOS and WM-ICOS for various spectrometer designs is then crucial to determine in what cases wavelength modulation can provide a substan-

Table 1 Summary of various WM-ICOS SNR enhancements reported in the literature and the key experimental parameters corresponding to each

Reference	*SNR* Enhancement	Mirror reflectivity	Cavity length (m)	*WM* frequency (kHz)	λ (nm)
Zhao [6]	14	0.993	0.44	12	1573
Jia [7]	9.17	0.9969	0.358	?	1531
Kasyutich [8]	7	0.998	0.22	10	670
Bakhirkin [9]	5	0.99975	0.5	50	5450
Bakhirkin [10]	5	0.99975	0.053	5	5200

P. Malara (✉) · M.F. Witinski · F. Capasso · J.G. Anderson
School of Engineering and Applied Sciences, Harvard University, Cambridge, MA 02138, USA
e-mail: pietro.malara@ino.it

F. Capasso (✉)
e-mail: capasso@seas.harvard.edu

M.F. Witinski
Eos Photonics, Inc., Cambridge, MA 02142, USA

P. Malara · P. De Natale
Consiglio Nazionale delle Ricerche - Istituto Nazionale di Ottica, and European Laboratory for Nonlinear Spectroscopy (LENS), Via Campi Flegrei 34, 80078 Pozzuoli (Naples), Italy

tial SNR improvement, that is, an improvement which would otherwise not be achievable by simply using a higher finesse cavity or a more sensitive detector.

The ICOS technique is typically based on an off-axis cavity alignment. In this geometry, the beam displaces at every reflection, drawing an elliptical pattern on the cavity mirrors, and traces back its original trajectory only after a number m of round trips. The free spectral range (FSR) is then compressed to $FSR_{\text{eff}} = c/2mL$, where L is the mirror separation [15, 16]. When the FSR_{eff} reduces to less than the laser linewidth, for any laser frequency, there will always be a certain amount of radiation coupled to the cavity, which in fact starts to behave as a nonresonant object. The off-axis alignment therefore dramatically reduces the cavity's resonance fluctuations, providing a smoothed average transmission that is particularly useful in spectroscopy, where small absorption signals need to be resolved from the baseline cavity transmission.

Off-axis injection of cw lasers allows the behavior of laser light in the cavity to be described by a simple rate equation. Considering a cavity of length L, mirror reflectivity R, with a constant incident radiation intensity I_0, and which contains a sample with per-pass absorption A. The per-pass intensity loss is $dI = -I(1 - R + A)$ while the per-pass optical transit time is $dt = L/c$. If the number of passes is large and dI is small, the ratio between these two quantities can be written as a differential equation [16]:

$$\frac{dI}{dt} = \frac{c}{2L}\left[I_0 CT - 2I(1 - R + A)\right] \tag{1}$$

where the source term $I_0 CT$ represents the average cavity injection. (C is a coupling parameter between 0 and 1 and T is the input mirror transmittance.) The steady-state solution of Eq. (1) multiplied by T gives the average off-axis cavity transmission:

$$I_t = \frac{I_0 CT}{2(1 - R + A)} T \tag{2}$$

Equation (2) can be used to calculate the fractional absorption, resulting in a simple Beer–Lambert-like relationship where a factor proportional to the cavity finesse $\Im$ is gained in the interaction path length. Indeed, ICOS is unique in that it maintains this path length enhancement which is common to all cavity enhanced techniques, while providing an intrinsic insensitivity to small vibrations and misalignments.

In Eq. (2), the incident intensity values I_0 and the coupling parameter C are the only dynamic quantities, and can be considered as average values with fluctuations δI_0 and δC, respectively. Fluctuations of C are chiefly responsible for the incomplete flattening of the cavity resonance structure. This noise is primarily caused by the random nature of the injection of a laser into a cavity mode. Intuitively, it can be seen as originating in the fast jittering of the optical frequency inside the laser linewidth, which may instantaneously overlap more or less completely with the cavity resonance profile [14].

In an axial cavity alignment, as the laser scans through the TEM_{00} cavity modes, the coupling efficiency is well described by a Poissonian distribution with mean value $\overline{C_a}$ and variance $\delta C_a = \sqrt{\overline{C}_a}$ [17]. The actual value of the average resonant coupling strongly depends on the "passage in resonance" dynamics, which are defined by the cavity mode and laser linewidths ($\gamma_{\text{cav}}, \gamma_{\text{las}}$) and by the scan velocity used. For sufficiently fast scans, typical of the ICOS techniques, $\overline{C}_a \approx \frac{\gamma_{\text{cav}}}{\gamma_{\text{las}}}$ [17].

In an off-axis alignment, a number $N = \gamma_{\text{las}}/FSR_{\text{eff}}$ of cavity modes fall within the laser linewidth, and are therefore injected simultaneously. Considering these injection events as independent, the coupling efficiency can be extended to the off-axis case by simply considering a mean value $\overline{C} = N\overline{C}_a$ and a variance $\delta C = \frac{\sqrt{\overline{C}_a}}{\sqrt{N}}$. Substituting the expressions for $\overline{C}_a$ and N, and using the relation $\gamma_{\text{cav}} = \frac{FSR}{\Im}$, we obtain the following expression for the average mode coupling and its fluctuation in an off-axis cavity:

$$\bar{C} = \frac{\gamma_{\text{cav}}}{FSR_{\text{eff}}} = \frac{m}{\Im} \tag{3a}$$

$$\delta C = \sqrt{\frac{\overline{C}_a}{N}} = \sqrt{\frac{\gamma_{\text{cav}} FSR_{\text{eff}}}{\gamma_{\text{las}}^2}} = \frac{\gamma_{\text{cav}}}{\gamma_{\text{las}}}\sqrt{\frac{\Im}{m}} \tag{3b}$$

Finally, propagating the error with respect to C in Eq. (2), we get the baseline intensity noise due to the coupling fluctuations (mode injection noise):

$$\Delta I_{\text{opt}}(R) \approx \frac{I_0 T^2}{2(1 - R)} \delta C \tag{4}$$

In general, the mode injection noise is not the only optical noise source in ICOS. Indeed, in any practical off-axis alignment, the finite laser spot size causes partial overlapping of the beam before the re-entrant condition is met. As a consequence, unwanted etalon interferences arise, which can mask weak absorption signals. This type of optical noise can be largely reduced by improving the alignment or using large diameter mirrors [19]. For this reason, we chose to neglect it in our analysis.

Optical noise in ICOS is mainly reduced by using a fast scan of the laser wavelength across the cavity modes and time integration of the transmitted signal. In fact, with a scan velocity ν_{scan} (Hz/sec) and a time integration t, the coupling C is further averaged over $K = \frac{\nu_{\text{scan}} t}{FSR_{\text{eff}}}$ cavity modes [14]. In both ICOS and WM-ICOS, this averaging effect reduces the mode injection noise by an additional factor $1/\sqrt{K}$, the only difference being that in WM-ICOS the role of ν_{scan} is

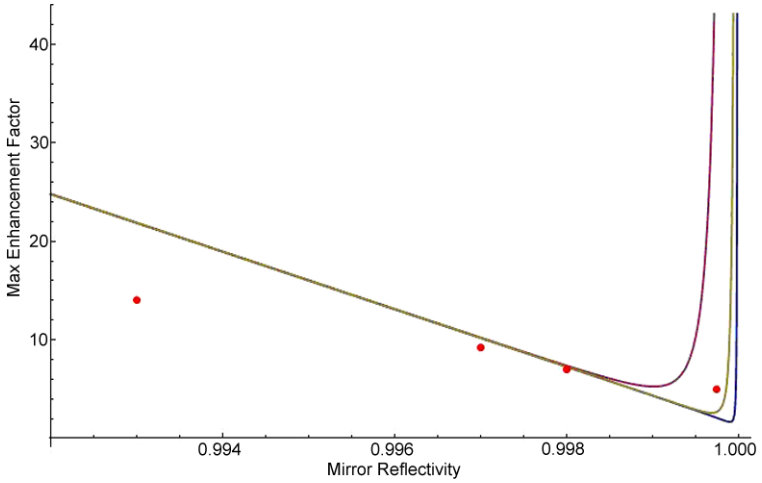

Fig. 1 Sensitivity enhancement factor attainable in ICOS after the complete suppression of the electronic $1/f$ noise, plotted as a function of R. Different curves correspond to different detector noise levels: $\delta I_{\mathrm{det}} = 10^{-8}$ (*purple*), 10^{-9} (*green*), and 10^{-10} (*blue*). The following spectrometer parameters were adopted for all model curves: cavity length $L = 0.5$ m, transmission $T = 0.5(1 - R)$, off-axis reentrant condition $n = 1000$. Laser linewidth $\gamma_{\mathrm{las}} = 3$ MHz, fluctuations $\delta I_0 = 1$ % of laser amplitude, $\nu_{\mathrm{scan}} = 20$ GHz/sec, integration time $t = 100$ μs. The red spots correspond to the WM-enhancement values reported in literature (see Table 1)

played by the wavelength modulation. As we will point out in next section, the scan velocity cannot be increased indefinitely in either ICOS or WM-ICOS, due to the emergence of a nonnegligible "skew" of the spectral features of interest [5, 6, 18].

The noise contributions from the laser source fluctuations (δI_0) and the detector/preamplifier noise (δI_{det}) also have to be taken in account. The former is obtained by differentiating Eq. (2) with respect to I_0, whereas the latter is a noise floor that is independent of the optical cavity characteristics.

We can finally obtain the overall noise level of an ICOS signal by combining in quadrature all the above described noise sources:

$$\Delta I_{\mathrm{tot}}(R) = I_0 \sqrt{\left(\frac{T^2}{2(1-R)}\delta C\right)^2 + \left(\frac{\overline{C}T^2}{2(1-R)}\frac{\delta I_0}{I_0}\right)^2 + \left(\frac{\delta I_{\mathrm{det}}}{I_0}\right)^2} \tag{5}$$

It is worth noting that if we express I_0 in power units, then the last term $\delta I_{\mathrm{det}}/I_0$ is equivalent to the ratio between the detector noise equivalent power (NEP) and the laser power incident on the cavity.

The last two terms of Eq. (5) are crucial for WM-ICOS. Indeed, as we mentioned before, the optical noise is averaged out in the same way by the fast scan in ICOS and by the fast modulation in WM-ICOS. The additional SNR enhancement of WM-ICOS then relies on the fact that the modulation/demodulation process encodes the signal in a narrow electrical bandwidth away from DC, where the non-optical noise (that usually scales as $1/f$) is reduced.

In Fig. 1, we show a plot of $\Delta I_{\mathrm{tot}}/(\Delta I_{\mathrm{tot}} - \Delta I_{\mathrm{el}})$ vs. R, where ΔI_{el} is the quadratic sum of the last two terms of Eq. (5). This function represents the SNR enhancement due to the complete suppression of the $1/f$ noise in the ICOS signal, and can in fact be thought as the theoretical limit to the improvement obtainable by WM-ICOS over ICOS. To plot this function for a given spectrometer, a detailed knowledge of all the laser ($I_0, \delta I_0, \gamma_{\mathrm{las}}$), the cavity ($m, T, L$) and the detector ($\delta I_{\mathrm{det}}$) parameters are needed. However, in order to allow a reasonable comparison with the values of Table 1, which were obtained with different spectrometers, we used a set of average parameters (listed in the figure caption) for an optimized off-axis ICOS spectrometer.

It is important to notice that although with a different offset or slope, for any set of reasonable parameters used, the electronic noise fraction (and thus the possibility of WM improvement) of the ICOS output decreases with R, until very high R are approached. Such a behavior well reproduces the trend depicted by the results of Table 1 (superimposed as red spots in Fig. 1), and indicates that, as a general rule, it is harder to obtain a significant WM enhancement in a high-finesse ICOS setup, unless the finesse is so high that the detector noise dominates.

In particular, three key regions can be identified in Fig. 1. At low mirror reflectivity (below 0.998), because of the relatively high transmission, the laser amplitude fluctuations dominate the overall noise level. A high sensitivity improvement is attainable in this region regardless of δI_{det}. For higher values of R (0.998–0.9995), the cavity throughput is reduced, so optical and electronic noise contributions are more balanced. As a consequence, the δI_{det} dependence starts to be critical. Finally, at ultrahigh reflectivity, when

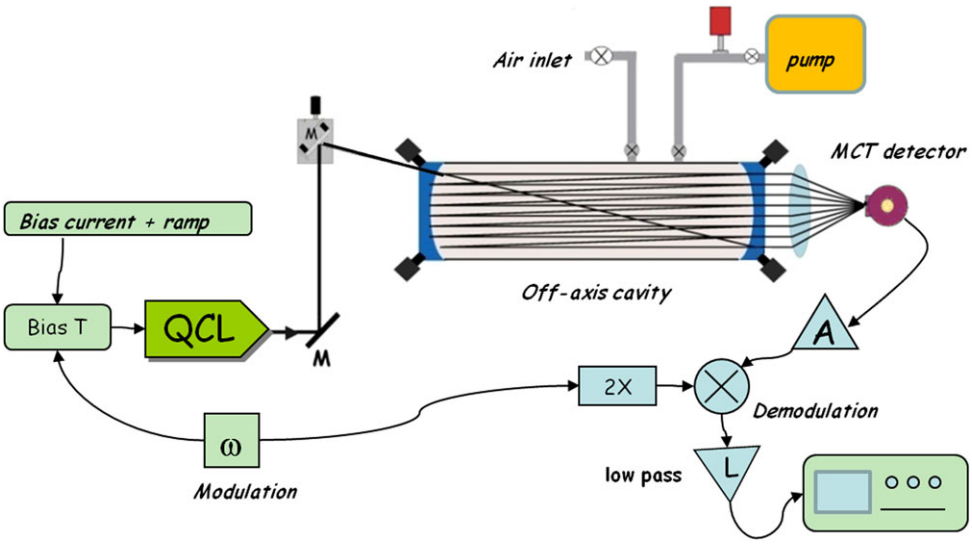

Fig. 2 Experimental setup for the comparison between ICOS and WM-ICOS performance in ambient-air methane isotopologue detection

the cavity transmission gets close to the detector's NEP, the detector's noise becomes the limiting factor. Only after this "inversion point" WM could provide a dramatic enhancement on top of an already ultrasensitive spectrometer.

2 Experimental apparatus

In order to compare the performances of ICOS and WM-ICOS experimentally, we added WM capability to an existing high sensitivity ICOS experiment. A full description of the experimental apparatus is given in [5, 18] and we note only certain features here as well as the added WM-ICOS electronics. The modified setup could be run in ICOS, WM-ICOS, and cavity ringdown mode and is sketched in Fig. 2. The light source was a thermoelectric cooled DFB quantum cascade laser (QCL) delivering a power of around 10 mW at the target wavelength of 1294 cm^{-1}. The laser current was supplied by the summed output of the DC and AC electrical components, which were combined at a bias tee (Minicircuits 3434). At the DC port of the bias tee, we introduced both a small offset current and a sawtooth ramp (10–1000) Hz for scanning over the spectral line of interest while remaining constantly above threshold.

At the bias tee, these two slower components were summed with the higher frequency AC component which was used for wavelength modulation. The $L = 90$ cm cavity with air inlets and outlets was equipped with two custom coated 10 cm diameter ZnSe mirrors, with a typical reflectivity of 0.9996 at 1294 cm^{-1} (measured by cavity ringdown at the beginning and end of every experimental run) and curvature radius of 140 cm. The cavity transmission is focused on a nitrogen-cooled DC-coupled photovoltaic MCT detector with $D^* = 10^{10}$. By turning off the modulation and bypassing the mixer, both ICOS and WM-ICOS spectra could be acquired in the same conditions for a direct comparison. It is worth noting that using a photovoltaic detector, which is not affected by the $1/f$ noise, represents the best choice for the direct ICOS technique, where a DC signal has to be measured. A higher WM-enhancement could in principle be achieved with a photoconductive detector. However, since extremely sensitive photovoltaic MCTs are nowadays commercially available, using such a detector yields a more realistic comparison of the two techniques.

3 Acquisition strategies and results

As we mentioned in the previous paragraph, increasing the scanning speed increases the achievable SNR in ICOS. In fact, a faster scan provides a twofold advantage: on one hand it reduces the optical noise as discussed in previous section, while on the other allows for the averaging of more spectra in the same acquisition time. The upper limit to the useful scan speed is set by the emergence of line skew, as thoroughly discussed in [5, 18]. Such a limit for ICOS is generally around several hundreds of Hz. In comparison, the maximum scan speed that can be used in WM-ICOS is dramatically lower for the following reason:

Consider a radiation whose wavelength is modulated as $\omega(t) = \omega_0 + a\cos(\omega_m t)$ interacting with a weakly absorbing medium of length L and absorption coefficient $\alpha(\omega)$. The transmitted intensity is

$$I\big(\omega_0(t)\big) = I_0\big(1 - \alpha(\omega_0 + a\cos\omega_m t)L\big) \tag{6}$$

Such a signal, periodic in ω_m, can be expanded in a Fourier series. When demodulating (at $\omega_m, 2\omega_m$) with a lock-in amplifier or with a mixer+lowpass filter, one retrieves the corresponding (1^{st}, 2^{nd}) Fourier coefficient of this

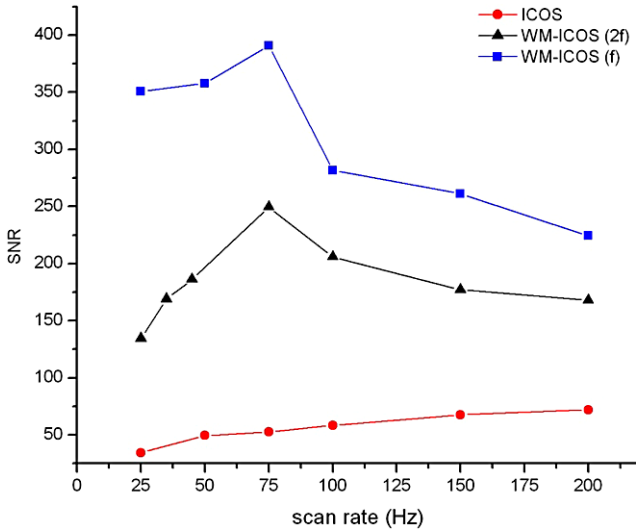

Fig. 3 SNR of the CH_4 line @ 1294.38 cm^{-1} in a sample of 13 Torr ambient air obtained for different scan rates by ICOS (*red*) and WM-ICOS (f signal = *blue*, $2f$ signal = *black*)

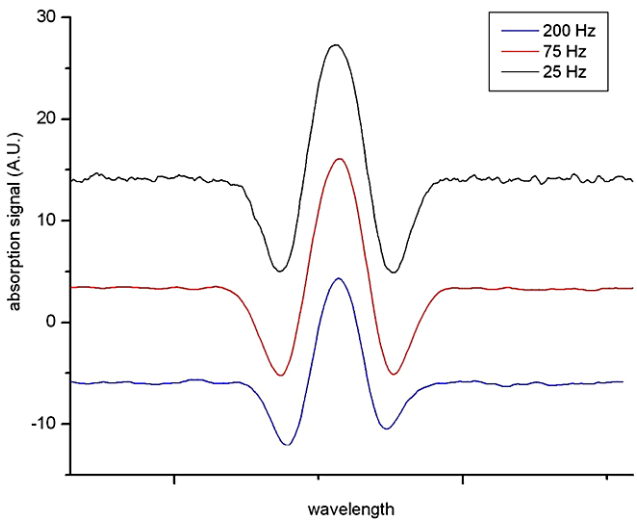

Fig. 4 Examples of WM-ICOS 2f signals (512 averages) at three different scan rates. For small values of ν_{scan} (*black line*), there is lot of residual baseline noise, while for scans as fast as 200 Hz (*blue line*) the lineshape shows clear signs of distortion. An optimal scan rate of 75 Hz was found for our setup

expansion. For example, the second coefficient:

$$H_2(\omega_0) = \int_0^{\pi} I\big(\omega_0(t)\big) \cos 2\omega_m t \, d\omega_m t \tag{7}$$

From Eq. (7), it can be seen that to compute an accurate value of the transmission at a frequency ω_0 with wavelength modulation, it takes half of one modulation cycle. This requirement poses severe limitations when wavelength modulation is used in conjunction with fast scan rates, like in ICOS.

Indeed, when a regular scan across an absorption line is performed at a rate ν_{scan}, and digitized in a number P of points by a DAQ card, each spectral point is acquired in a time $\Delta t_{scan} = 1/P\nu_{scan}$. When using WM instead, a minimum time $\Delta t_{WM} = \pi/\omega_m$ is required to compute the integral of Eq. (7). As a consequence, there emerges a critical scan rate that satisfies the condition $\Delta t_{scan} = \Delta t_{WM}$, at which each spectral point is calculated independently by WM. For scan rates faster than this, the laser will be probing the next spectral point before the integral of Eq. (7) is completed, thus introducing a distortion in the digitized spectrum. With a 16 k Hz modulation and a digitization $P = 500$ points per scan, the critical scan rate is $\nu^* = 2\nu_m/P = 64$ Hz.

In Fig. 3, we show the measured SNR for the CH_4 absorption line at 1294.38 cm^{-1} in 13 Torr ambient air, acquired respectively by ICOS and WM-ICOS (f and $2f$ demodulations) at 16 k Hz. The optimal modulation conditions were found empirically by optimizing the demodulated signal. In particular, the best modulation index resulted to be different for the f and the $2f$ WM signal (probably because of the cavity low-pass filter that attenuates the $2f$ output).

The signal was measured as the peak-to-baseline voltage, while the noise level was calculated as the standard deviation of the baseline (acquired in a region with no absorption lines).

As can be seen in Fig. 3, the quality of the WM-ICOS is constantly higher than the regular ICOS, reaching a peak value of 391 @ 75 Hz and degrading rapidly for higher scan rates. An example of how the WM-ICOS signal appears at different scan rates is shown in Fig. 4 for the $2f$ demodulation.

As opposed to that, the ICOS SNR increases with the scan rate, reaching a plateau at 250–300 Hz with SNR around 80, and slowly getting worse only for scan rates beyond 500 Hz. Therefore, a fair comparison should be carried on using the best signals obtainable with the two techniques, namely between ICOS @ 500 Hz and WM-ICOS @ 75 Hz.

All the data in Fig. 3 were acquired in the conditions of minimum electrical bandwidth. That is, at every scan the lowest low-pass filter that did not distort the signal was used (1–3 k Hz, 6 dB/oct for WM and 10–30 k Hz for ICOS). A bandwidth-normalized comparison yields in this case a WM enhancement never higher than 1.5.

However, bandwidth normalization is meaningful only in the assumption of Gaussian noise, which is not true in any high finesse ICOS measurement, where the optical noise is still dominant. In this case, a more practical evaluation of the detection capability of the two techniques can be carried on by minimizing empirically the electrical bandwidth, and then comparing the signal to noise ratios obtainable in 1 sec

averaging. In this way, from the data of Fig. 3, we get

$$\frac{SNR_{wm-i\cos}^{75\ \mathrm{Hz}}}{SNR_{i\cos}^{500\ \mathrm{Hz}}}\sqrt{\frac{75}{500}} = \begin{cases} 1.9 \\ 1.2 \end{cases}$$

for the f and $2f$ signals, respectively.

In any case, in our analysis, the WM-ICOS technique results only marginally more sensitive than conventional ICOS. Such a small enhancement can is a clear sign that our spectrometer is not limited by electronic noise. The reduced effectiveness of WM can be also addressed to the high slope efficiency of the QCL, introducing a large amount of residual amplitude modulation noise (RAM).

However, the above expression points out a general limitation of the WM technique, namely, its necessarily slow scan rate compared to regular ICOS. In our interpretation, the limitation in the scan rate is caused by the finite amount of time needed to compute the integral of Eq. (7) for each spectral point. The WM scan rate could be then improved only by increasing the modulation frequency. However, because of the cavity low-pass, increasing the modulation frequency means increasing its amplitude consequently, at a rate of 6 db/oct.

We next ran a second set of measurements at a reduced laser power (from 10 to 2.5 mW). In this way, we selectively increased a noise source that can be reduced by WM (third term of Eq. (5)). Wavelength modulation is therefore expected to have a more positive effect on SNR, although a quantitative prediction would require accurate measurements of the spectrometer noise levels in Eq. (5).

Under the low laser power conditions, we could indeed observe a 20–30 % better enhancement for WM-ICOS. The 500 Hz ICOS and the 75 Hz f and $2f$ signals dropped, respectively, to SNR values of 53, 320, and 218. Our effective comparison yields in this case $SNR_{wm-i\cos}/SNR_{i\cos} = 2.3$ for the f and 1.6 for the $2f$ signal.

Finally, we calculate for our WM-ICOS setup the minimum detectable absorption coefficient in 1 sec averaging. From our data, taken with scan rate $\nu_{\mathrm{scan}} = 75$ Hz at a pressure $P = 13$ Torr and a number of averages $N_{\mathrm{ave}} = 532$, we get

$$\alpha_{\min} = \sigma_{\min} n = \frac{S(T)}{SNR\sqrt{\frac{\nu_{\mathrm{scan}}}{N_{\mathrm{ave}}}}\cdot \pi\gamma_{\mathrm{air}}(P)} N_L(P,T)\bar{n}P$$

$$= \begin{Bmatrix} 2.75\times 10^{-10} \\ 1.45\times 10^{-10} \\ 2.28\times 10^{-10} \end{Bmatrix} \mathrm{cm}^{-1}\ \mathrm{Hz}^{-1/2}$$

for respectively the ICOS and the WM-ICOS f and $2f$ signals. The line strength $S(T)$ and the air broadening coefficient γ_{air} values for the given CH_4 absorption line were provided by the HITRAN database, $N_L(P,T) = P/K_bT$ is the Loschmidth number at 13 Torr and ambient temperature, and $\bar{n}$ is the average methane concentration in air (1.8 ppm).

4 Conclusions

The added value that wavelength modulation can actually bring to the ICOS technique is strongly dependent on a number of spectrometer variables: the optical cavity design and the scan rate, as well as the laser, detector, and preamplifier used. We proposed a simple way to model the various contributions to the overall noise level in an ICOS spectrometer that allows estimating the maximum SNR enhancement attainable by application of WM. According to our model, for cavity finesses normally used in ICOS spectrometers this quantity decreases as the mirror reflectivity increases. As a consequence, the higher the ICOS cavity finesse, the harder is to improve the detection sensitivity using a wavelength modulation technique. This behavior is qualitatively in good agreement with the results reported in the existing WM-ICOS literature. However, by further increasing the cavity mirror reflectivity, the model predicts again a dramatic impact of WM on the ICOS detection sensitivity. Normally, it is not convenient to use such a high finesse cavity in an ICOS spectrometer, because the transmission is so low that the advantage of having a longer absorption path length is neutralized by the increased electronic noise level [18]. Instead. according to the presented model, the wavelength modulation technique could allow to fully profiting the use of ultrahigh finesse cavities in ICOS spectrometers.

We finally carried on a thorough experimental comparison between ICOS and WM-ICOS in ambient-air methane detection using an high-sensitivity ICOS-optimized setup. We found that practical application of the WM-ICOS technique is chiefly limited by its necessarily slow acquisition rate compared to that of the traditional technique, confirming another point put in evidence by our theoretical analysis. In fact, WM did provide an appreciable sensitivity improvement (a factor 7.5) only for slow scan frequencies. As the scan rate was increased, WM-ICOS signal degraded, while regular ICOS SNR kept on improving. This reduced averaging capability strongly affects WM-ICOS effectiveness. Ultimately, the direct comparison between the two techniques yielded a factor 2 enhancement by WM. A second set of measurements was carried on at a lower laser power, to simulate a reduced transmission cavity. According to the model, the WM enhancement increased. In conclusion, by pointing out the main advantages and the limitations of the WM-ICOS technique, we believe that the proposed analysis can provide useful guidelines to design a WM- ICOS optimized spectrometer.

References

1. J.B. Paul, L. Lapson, J. Anderson, Appl. Opt. **40**, 4904 (2001)
2. S. Williams, M. Gupta, T. Owano, D.S. Baer, A. O'Keefe, D.R. Yarkony, S. Matsika, Opt. Lett. **29**, 1066 (2004)

3. P. Malara, P. Maddaloni, G. Gagliardi, P. De Natale, Opt. Express **14**, 1304 (2006)
4. M.L. Silva, D.M. Sonnenfroh, D.I. Rosen, M.G. Allen, A. O'Keefe, Appl. Phys. B **81**, 705 (2005)
5. M.F. Witinski, D.S. Sayres, J.G. Anderson, Appl. Phys. B (2010). doi:10.1007/s00340-010-3957-2
6. W. Zhao, X. Gao, W. Chen, W. Zhang, T. Huang, T. Wu, H. Cha, Appl. Phys. B **86**, 353 (2007)
7. H. Jia, X.-y. Guo, T. d. Cai, W.-x. Zhao, L. Wang, T. Tan, W.-j. Zhang, X.-m. Gao, Spectr. Spectr. Anal. 29(12), 3173–3176
8. V.L. Kasyutich, C.E. Canosa-Mas, C. Pfrang, S. Vaughan, R.P. Wayne, Appl. Phys. B **75**, 755 (2002)
9. Y.A. Bakhirkin, A.A. Kosterev, C. Roller, R.F. Curl, F.K. Tittel, Appl. Opt. **43**, 2257 (2004)
10. Y.A. Bakhirkin, A.A. Kosterev, R.F. Curl, F.K. Tittel, D.A. Yarekha, L. Hvozdara, M. Giovannint, J. Faist, Appl. Phys. B **82**, 149 (2006)
11. R. Vasudev, Appl. Phys. B **87**, 163 (2007)
12. Z. Tan, X. Long, X. Feng, Z. Wei, Opt. Commun. **284**, 852 (2011)
13. W. Zhao, X. Gao, L. Hao, M. Huang, T. Huang, T. Wua, W. Zhang, W. Chen, Vib. Spectrosc. **44**, 388 (2007)
14. A. Zybin, Y.A. Kuritsyn, V.R. Mironenko, K. Niemax, Appl. Phys. B **78**, 103 (2004)
15. D.R. Herriott, H. Kogelnik, R. Kompfner, Appl. Opt. **3**, 523 (1964)
16. P. Maddaloni, G. Gagliardi, P. Malara, P. De Natale, J. Opt. Soc. Am. B **23**, 1938 (2006)
17. J. Morville, D. Romanini, M. Chenevier, A. Kachanov, Appl. Opt. **41**, 6980 (2002)
18. E.J. Moyer, D.S. Sayres, G.S. Engel, J.M. St. Clair, F.N. Keutsch, N.T. Allen, J.H. Kroll, J.G. Anderson, Appl. Phys. B **92**, 467 (2008)
19. G.S. Engel, W.S. Drisdell, F.N. Keutsch, E.J. Moyer, J.G. Anderson, Appl. Opt. **45**, 9221 (2006)